Distribution Agreement

In presenting this thesis as a partial fulfillment of the requirements for a degree from Emory University, I hereby grant to Emory University and its agents the non-exclusive license to archive, make accessible, and display my thesis in whole or in part in all forms of media, now or hereafter now, including display on the World Wide Web. I understand that I may select some access restrictions as part of the online submission of this thesis. I retain all ownership rights to the copyright of the thesis. I also retain the right to use in future works (such as articles or books) all or part of this thesis.

Tianshu Huang April 3, 2020

Testing the Charge Residence Time on Acoustically Levitated Particles

by

Tianshu Huang

Justin Burton
Advisor

Department of Physics

Justin Burton
Advisor

Alessandro Veneziani
Committee Member

Effrosyni Seitaridou
Committee Member

2020

Testing the Charge Residence Time on Acoustically Levitated Particles

by

Tianshu Huang

Justin Burton
Advisor

An abstract of
a thesis submitted to the Faculty of Emory College of Arts and Sciences
of Emory University in partial fulfillment
of the requirements of the degree of
Bachelor of Science with Honors

Department of Physics

2020

Abstract

Testing the Charge Residence Time on Acoustically Levitated Particles

by Tianshu Huang

Triboelectric charging on moving particles is widely observed in nature. Studies have discovered the effects of both size and material type on the polarity and charge density of charged particles, and the mechanisms by which the particles get charged. Meanwhile, little is known about the stability of charge on the particle. One main issue for testing a particle's discharge behavior comes from the difficulty in controlling the potential influencing factors. Getting into contact with other objects can cause charge variation on the particle. Many charge measurement methods may also provide additional pathways for charge transfer.

In our thesis, we use a charge-sensing acoustic levitator to explore the discharge behavior of polystyrene bead. We test the levitation performance on pumice and polystyrene bead in different air pressure conditions. We find that, for a spherical particle of a given size, the acoustic radiation force required to levitate the particle is proportional to the particle's density and air density. Using polystyrene bead as test particles, we measure the discharge process in different relative humidities. We discover that the charge can be retained for weeks at low humidity, but decays in a few hours at high humidity. The charge loss follows a logistic behavior, which indicates that there may exist a two-step charge loss process. We also perform the measurement on gold bead and discover that the composition of the particle doesn't play a major role in the discharge behavior. Future investigation focuses on taking measurements under different pressure condition and gas compositions.

Testing the Charge Residence Time on Acoustically Levitated Particles

by

Tianshu Huang

Justin Burton
Advisor

A thesis submitted to the Faculty of Emory College of Arts and Sciences
of Emory University in partial fulfillment
of the requirements of the degree of
Bachelor of Science with Honors

Department of Physics

2020

Acknowledgements

I would like to express my great appreciation to my advisor Dr. Justin Burton, who offered this great opportunity to work on the project, for his professional guidance and valuable support. I would like to offer my special thanks to Dr. Joshua Méndez Harper, for his patient guidance, enthusiastic encouragement and the constructions of the experiment setup. I wish to acknowledge the help provided by Jake McGrath, who helped to construct and test the second setup, and performed experiments on the water layer' thickness; and Yannic Gagnon, who helped to construct the QCM.

Contents

Chapter 1

Introduction

Particle charging occurs in a wide range of natural phenomena, from small activities in daily life (taking off the sweater in winter) to large geophysical (dust devil, storms) and planetary systems (planet atmosphere), and plays a critical role in them. Triboelectric charging, a charging processs on which particles can be electrically charged by contacting other particles, is one of the main sources of electrification. The triboelectric charging in dust storms and dust devils on Mars [1] has a significant impact on Mars' planetary environment [2][3]. It stimulates chemical reactions, such as the dissociation of methane and production of hydrogen peroxide, which change Mars' atmosphere. Such phenomena account for the organic degradation [4] and create sharp-edged razorbacks on Mars' surface [5]. The charging effect has an important effect on the evolution of life on Earth [6]. For example, as volcano erupts, lighting occurs in the volcanic plumes [7]. A volcanic lighting accelerates the process of nitrogen fixation and increases the concentration of reduced gases (methane, ammonia) [8]. Such reduced gases are essential for synthesizing key chemical components to generate life.

While people have long recognized the triboelectric charging process and its effects, the underlying principles and mechanisms of discharging process are not well understood. Many studies focus on the charging processes, but little is known about the stability of charge on the particles.

In nature, charge on the particles may last a long period before interacting with other substances. Examining the stability of charge on particles would lead to new understandings of certain natural phenomena, and would bring new insights into studying the charging process too. This thesis will focus on measuring the discharging process and examining certain influencing factors.

One difficulty in studying the discharging process is to reduce the disturbance of other influencing factors and focus purely on the discharging process. In the natural environment, the interactions involved in the discharging process are complex. Many discharging environments are hard to reach (volcano eruptions, dust storms, upper atmosphere, Mars' surface). Moreover, measuring charge on the particle is also a big problem. Many measurement methods either require contacting a particle's surface or add additional pathways for charge to be transferred from the surface. To fully test the charge residence time on a particle, it is required that the particle needs to be isolated from contact and disruption during the entire experiments.

In our experiment, we use a novel, charge sensing acoustic levitator to control the movement of the particle and measure the charge on it. Acoustic waves carry energy and momentum as they travel through a medium. They can interact with obstacles along their paths and exert acoustic radiation forces on the obstacles. When the radiation force balances the object's weight, the object can be levitated. The acoustic levitator generates standing sound waves to levitate and trap particles. In this way, we can manipulate a particle's motion without physical contact.

Tada and Murata have tested the charge leakage on a steel ball (19mm diameter) suspended by Teflon fiber at high humidity [9]. They concluded that the charge loss is due to the direct leakage of charge into air, and discovered that charge decays faster at higher humidity. Their study provides insights on the effect of humidity on discharge behavior, but further investigations on the discharge mechanism in different humidity conditions are required. Triboelectric charging requires contact between particles, and equal amount of charges with opposite polarity are

distributed on the particles [10][11]. It is possible that the contact between charged and non-charged particles will lead to charge leakage. In our experiment, the test particle can only collide with air molecules. Since the air pressure affects the collision rate of air molecules, testing the discharge behavior at various pressures may also help understand the underlying mechanism. We will also show that the process of charge loss is distinctly different in dry and humid environments.

1.1 Acoustic radiation force

In this section we introduce the expression of acoustic radiation force generated by standing sound waves on a spherical particle [12][13][14]. By studying the maximum radiation force on the particle, we estimate the particle properties, such as size and density, required for the particle to be stably levitated.

Consider a spherical particle with radius a on the path of a sound wave with wavelength λ. Suppose that the particle is small ($a \ll \lambda$) and the wave is traveling in an inviscid fluid (i.e. the fluid has zero viscosity). The radiation force and radiation potential on the particle are given by

$$\vec{F_{rad}} = -\vec{\nabla} U_{rad}, \tag{1.1}$$

$$U_{rad} = \frac{4\pi}{3} a^3 \left[f_1 \frac{1}{2} \kappa_0 < p^2 > - f_2 \frac{3}{4} \rho_0 < v^2 > \right], \tag{1.2}$$

where κ_0 is the compressibility of the fluid; ρ_0 is the density of the fluid; $< p^2 >$ is the time average of the pressure field of the sound wave squared; $< v^2 >$ is the time average of the velocity field of the sound wave squared. The coefficient f_1 and f_2 are given by

$$f_1 = 1 - \frac{\kappa_p}{\kappa_0}, \tag{1.3}$$

$$f_2 = \frac{2(\rho_p - \rho_0)}{2\rho_p + \rho_0}. \tag{1.4}$$

where κ_p is the compressibility of the particle; ρ_p is the density of the particle.

In Equation (1.2), the term outside the parentheses denotes the volume of the spherical particle. As the sound wave propagates through the particle, the radiation force will both compress the particle and move the particle's position. The first term in the parentheses denotes the radiation potential from compressing a stationary particle; the second term in the parentheses denotes the radiation potential for a moving, incompressible particle. Since the compression force and transition force have opposite direction, the two terms has opposite sign.

The compressibility measures the change in volume as a response to a change in external pressure. Objects with high compressibility are easier to be compressed. In the radiation potential, f_1 denotes the coefficient of a stationary, compressible sphere in the propagating sound wave; f_2 denotes the coefficient of an incompressible sphere moving in the sound wave. If $\kappa_p = \kappa_0$, f_1 becomes zero; the radiation potential component from the incoming sound wave compressing the particle becomes zero. If $\rho_p = \rho_0$, f_2 becomes zero; there's no effect on the potential from the motion of the particle in the sound wave.

For a 1D planar wave traveling along z-axis in non-viscous fluid, the related pressure field, density field, and velocity field are given by

$$p(z,t) = p_a cos(kz) sin(\omega t), \tag{1.5}$$

$$\rho(z,t) = \frac{p_a}{c_0^2} cos(kz) sin(\omega t), \tag{1.6}$$

$$\vec{v}(z,t) = -\frac{p_a}{\rho_0 c_0} sin(kz) cos(\omega t)\hat{z}. \tag{1.7}$$

where c_0 is the speed of sound in the fluid; p_a denotes the amplitude of the pressure field.

Substituting Equation (1.5) and (1.7) to Equation (1.2), we obtain the radiation potential as

$$U_{rad} = \pi a^3 \kappa_0 p_a^2 [\frac{f_1}{3} cos^2(kz) - \frac{f_2}{2} sin^2(kz)]. \tag{1.8}$$

Here we use the fact that $\kappa_0 = 1/(\rho_0 c_0^2)$.

We then obtain the expression for radiation force by differentiating Equation (1.8) with respect to z.

$$\vec{F}_{rad} = \left[\frac{5\rho_p - 2\rho_0}{2\rho_p + \rho_0} - \frac{\kappa_p}{\kappa_0} \right] \frac{p_a^2}{4\rho_0 c_0^2} \frac{4\pi}{3} a^3 k sin(2kz)\hat{z}. \tag{1.9}$$

For hard particles like polystyrene and pumice in air, $\rho_0 \ll \rho_p$ and $\kappa_p \ll \kappa_0$. In this case, the term inside the parentheses in Equation (1.9) becomes $5/2$. Thus, Equation (1.9) is further simplified to

$$\vec{F}_{rad} = \frac{p_a^2}{\rho_0 c_0^2} \frac{5\pi}{6} a^3 k sin(2kz)\hat{z}. \tag{1.10}$$

The maximum radiation force is given by

$$F_{radmax} = \frac{20\pi^4}{3\lambda^3} \rho_0 c_0^2 d^2 a^3 \tag{1.11}$$

where λ is the wavelength of sound wave; d is the maximum displacement of air molecules. Here we used the fact that $p_a = c_0^2 \rho_0 d/\lambda$ and $\lambda = 2\pi/k$.

As Equation (1.10) presents, the radiation force is maximized at the antinodes (where $sin(2kz) = 1$) of the sound wave, and minimized at the nodes (where $sin(2kz) = 0$). We can manipulate a particle's levitated position by changing the relative phase of the sound wave.

Figure 1.1 shows how the particle can be levitated in the standing wave. At the position of the antinodes, the particle experiences maximum radiation force. The particle is then trapped in the space between two antinodes at the position of a node, where the radiation force is zero.

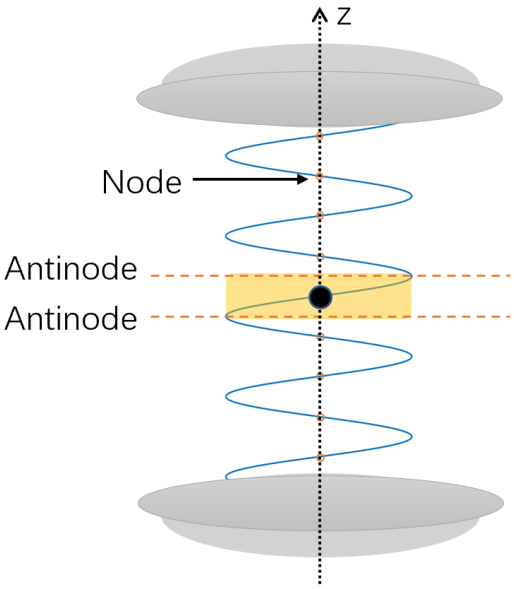

Figure 1.1: Demo of levitated particle inside the wave. The top and bottom gray plates is the wave emitter. The generated sound waves interfere and form standing waves between two plates. A spherical particle is trapped inside the yellow region, between the position of two antinodes

When the radiation force exceeds the gravitational force, the particle can be levitated. The minimum radiation force required to levitate the particle is given by:

$$mg = \frac{20\pi^4}{3\lambda^3}\rho_0 c_0^2 d^2 a^3 \tag{1.12}$$

Applying $m = 4/3\pi a^3 \rho_p$ for a spherical particle to Equation (1.2), we get

$$\rho_p g = \frac{5\pi^3}{\lambda^3}\rho_0 c_0^2 d^2 \tag{1.13}$$

From Equation (1.13), for a specific sound wave in a medium, the condition for levitating the particle is determined by the density of both the medium and the particle. For an ideal gas, the pressure is proportional to its density.

$$p = \rho RT \tag{1.14}$$

where p is the air pressure; ρ is the air density; R is the specific gas constant for that gas; T is the absolute temperature.

From Equation (1.14), as pressure decreases, the density decreases, and thus the radiation force decreases.

Chapter 2

Experiment

2.1 Design

2.1.1 Acoustic Levitator

We construct the acoustic levitator following the guide from Marzo et al. [15][16][17]. Our levitator is a single-axis non-resonant levitator. Figure 2.1 shows the general appearance of the levitator. The levitator consists of two hemispherical shells concaving towards each other. Each shell has 36 transducers. The 36 transducers are arranged in 3 circular rings with 6, 12 and 18 transducers (counting from the inner ring). The transducer operates at a frequency of 40kHz with a wavelength of 8.65mm. Each hemispherical shell serves as an emitter of the sound wave. The sound waves generated by the top and bottom emitters form standing waves in the space between the two emitters. The particle experiences the acoustic radiation force and can be levitated at the nodes.

We excite the transducers with sine waves. We use the Arduino Uno to control the sine wave signals to the transducers. By changing the phase difference between the sound wave from top and bottom emitters, we can adjust the position of the nodes and therefore move the particle.

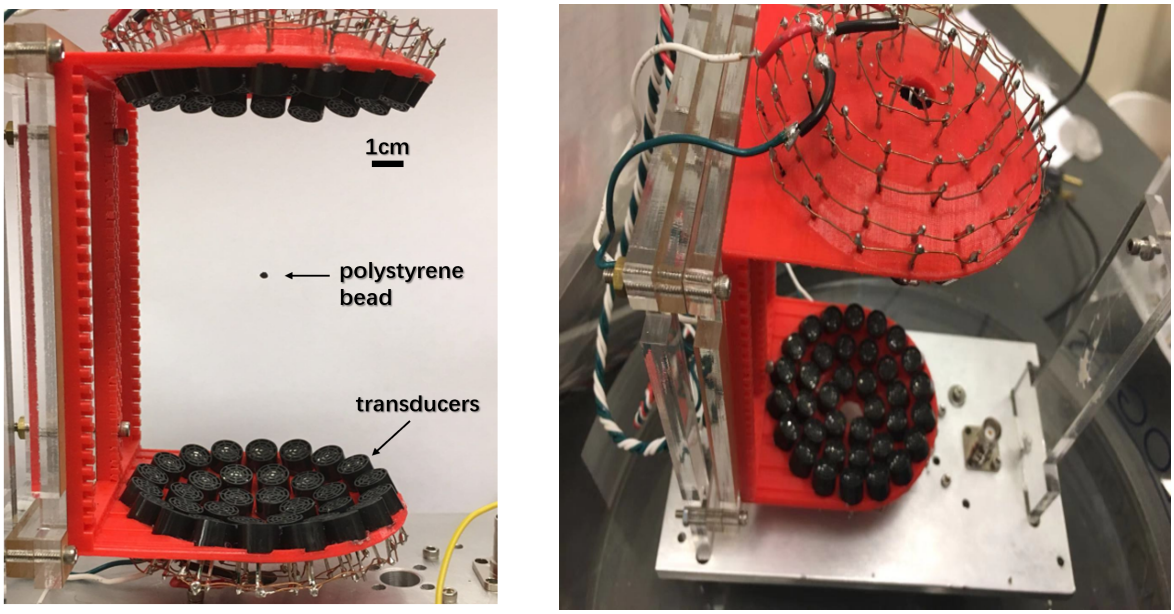

(a) (b)

Figure 2.1: Appearance of the acoustic levitator. Image (a) presents a polystyrene bead (radius = 1mm) levitated inside. Image (b) shows the arrangement of the transducers.

2.1.2 Charge Measurement Setup

Figures 2.2 and 2.3 show the experimental setup for charge measurement. We use the 10kV negative ion generator as the ionizer in the experiment; it's also controlled by Arduino Uno. A Faraday cup is placed inside the levitator for charge measurement. The Faraday cup is connected to a capacitor (C = 1000pF), resistor (R = 5GΩ) and a preamplifier together to measure the charge on the particle. By controlling the acoustic field inside the levitator, we can drop the particle into the cup and raise it again without contacting the cup's surface.

When we turn on the ion generator, it generates electron streams that negatively charge the levitating particle. Once the particle is charged, we lower the particle into the Faraday cup by changing the phase of the sound wave. As the negatively charged particle enters the cup, the repelled electrons in the RC circuit accumulate on the capacitor, creating a voltage difference across it. Knowing the capacitance, we can measure the voltage difference across the capacitor

and calculate the charge on the capacitors and, thus, on the particle.

We place the entire setup in a vacuum chamber with a small beaker inside. By controlling the amount of water and water temperature inside the chamber, we manipulate the humidity inside. We use the vacuum pump to control the pressure inside the chamber. The humidity and pressure are measured by sensors inserted in the vacuum chamber.

2.2 Procedures

2.2.1 Charge measurements

We first charge the particle, then measure the charge on it. We place the particle inside the levitator, right above the Faraday cup. During the charging process, we turn on the ion generator for 5 seconds, then turn it off. After that, we wait for 1 minute to allow any negative charge on the Faraday cup to dissipate. For a single measurement, we gradually drop the particle into the cup without contacting the bottom, wait for 1.5 seconds to detect charge differences, then raise the particle back to its original position. Between every single measurement, we wait for 1 minute. Depending on the relative humidity inside the chamber, the overall measuring time may last from a few hours to weeks. The 1min waiting time between two measurements are chosen to guarantee the charge on capacitor be completely dissipated.

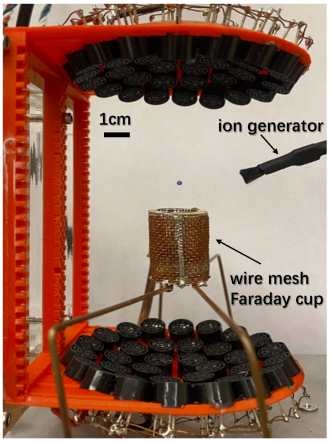

Figure 2.2: Actual figure of the charge measurement setup. A polystyrene bead is levitated inside the levitator. The ion generator shots electron streams to ionize the bead. The wire mesh Faraday cup can detect and measure the charge on the bead once it enters the Faraday cup.

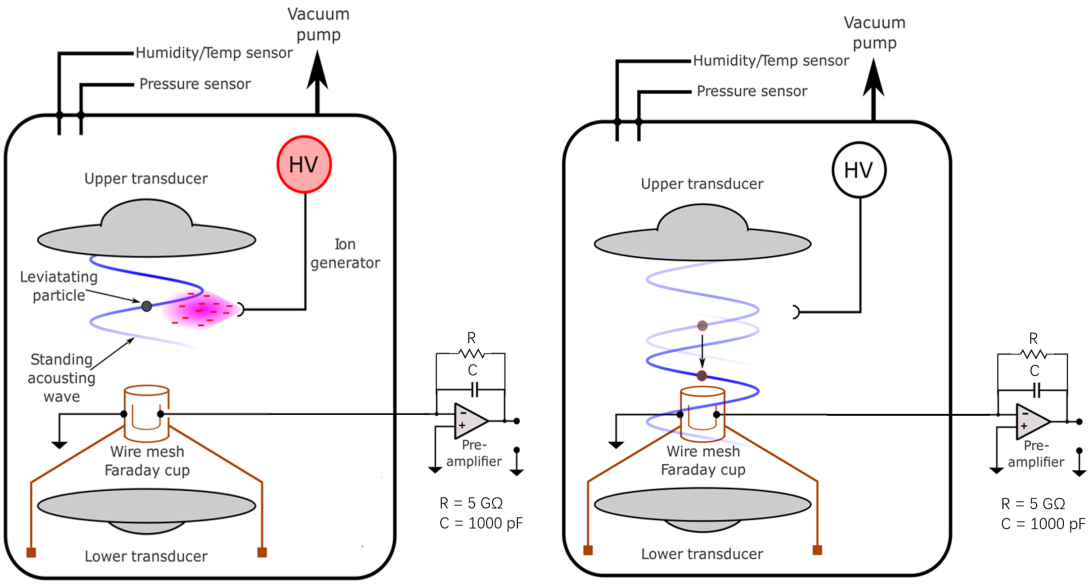

Figure 2.3: Schematic of experimental setup. Image (a) shows the charging process of the experiment. Image (b) shows the measurement process of the experiment.

Chapter 3

Results

3.1 Pressure variation

We test the performance of the levitator under various air pressures inside the chamber on different particles. We use two different particles for the experiment: polystyrene beads and pumice. The beads are spherical, expanded polystyrene foam with radius of 1mm. Such beads can be stably levitated at normal temperature and pressure (20°C, 1atm). The pumice is a silicon-based, rough textured volcanic glass. We use a 3D scanner to measure the volume of a large pumice rock and calculate its density. The testing pumice particles are small pieces of the large rock, cut in approximately the same size as the bead by hand.

For each material, we perform 20 experiments. As Equation (1.13) presents, when the pressure drops to a certain value, the radiation force will no longer hold the particle in air. In each experiment, we record the minimum air pressure at which the particle falls out of the acoustic trap. The mean value and standard deviation of the minimum pressure are listed in Table 3.1.

To further test the spatial extension of the acoustic trap, we measure the minimum pressure for multiple particles (number ranging from 1 to 9) levitated together in the levitator. We use

Particle	Density(g/cm^3)	Mean(kPa)	STD(kPa)	Size(mm)
Polystyrene Bead	0.0466	6.6	1.1	1
Pumice	0.299	33.2	5.6	

Table 3.1: Data of minimum pressure for each particle. Mean denotes the mean minimum pressure of 20 experiments. STD denotes the standard deviation. The density ratio of pumice to polystyrene bead is approximately 6; the mean minimum air pressure ratio is approximately 5. The polystyrene bead has a smaller standard deviation than pumice.

polystyrene beads to perform the experiment since the beads are levitated more stable than the pumice. The data is shown in Figure 3.1. As Figure 3.1 shows, the minimum air pressure

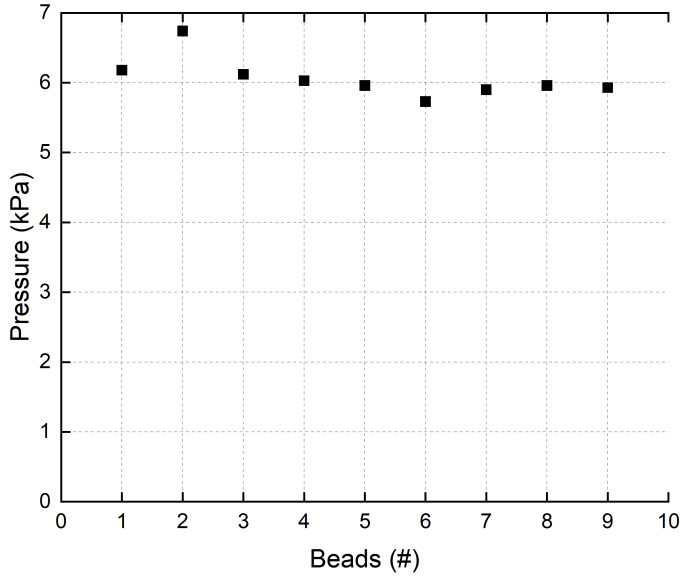

Figure 3.1: Minimum dropping pressure versus the number of beads levitated together. All the particles are levitated at the central node of the levitator. The particles are clustered in the same horizontal plane.

required for multiple particles is around 6 kPa. This is identical to the mean value for a single polystyrene bead in Table 3.1. Thus, the radiation force is large enough to levitate particles in such spatial extension.

3.2 Charge measurements

3.2.1 Sample measurement

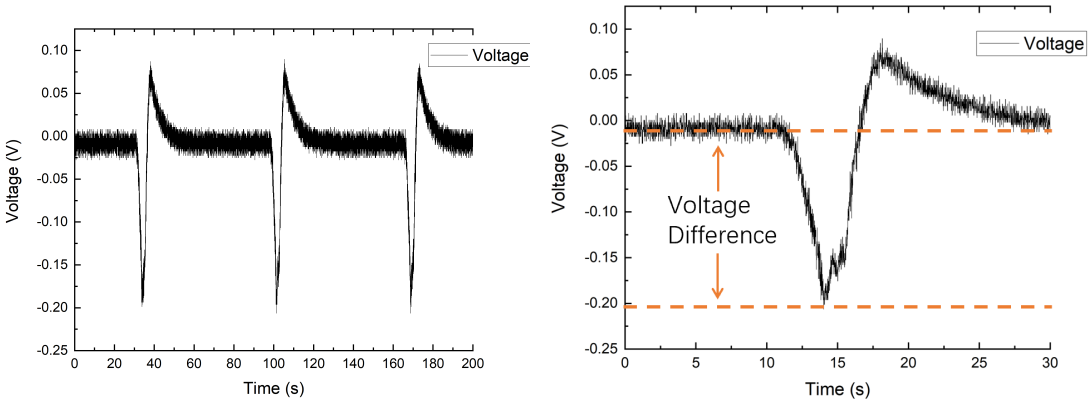

(a) (b)

Figure 3.2: A data sample of voltage changes collected from Faraday cup. Image (a) shows three identical measurement processes. Image (b) shows the detailed measurement for the second spike in image (a).

Figure 3.2 shows how the measured voltage changes across the capacitor as the particle enters and exits the Faraday cup. Initially, when the particle is levitated outside the cup, the voltage is approximately zero. The small fluctuations may be due to thermal noise. When the particle enters the cup from the top, the voltage drops, since the particle is negatively charged. As the particle exits the cup, the voltage increases to a positive value. Then, after waiting for 1 minute, the voltage drops back to zero, and we start a new measurement. The positive spike in Figure 3.2 is due to charge leakage through the resistor. Ideally, when the charged particle enters and exits the cup, the voltage would first drop to a certain value, then return to zero. When the particle stays in the cup for 1.5 seconds for the charge measurement, the resistor provides a path for a small amount of charge to escape. This creates a net positive voltage across the capacitor when the particle exits the cup.

We obtain the voltage difference by calculating the difference between the minimum voltage value and the baseline voltage (the voltage when no particle enters or exits the cup) in each measurement, as shown in Figure 3.2 (b).

3.2.2 Charge measurement as a function of humidity

We test the influence of humidity on a particle's discharging process. We use polystyrene beads as the testing particle for a more stable measurement. Our tested relative humidity (RH) ranges from 10% to 88%. For each relative humidity value, we perform the charge measurement for two days, calculate the voltage difference for each measurement, and plot the graph of voltage difference with respect to time.

We first study the particle discharging behavior for different RH values. Figure 3.3 shows two sample graphs of change in voltage difference with respect to time at 62% and 23% RH. These voltage difference measurements start at approximately the same value, and they represent the changes in both high and low RH.

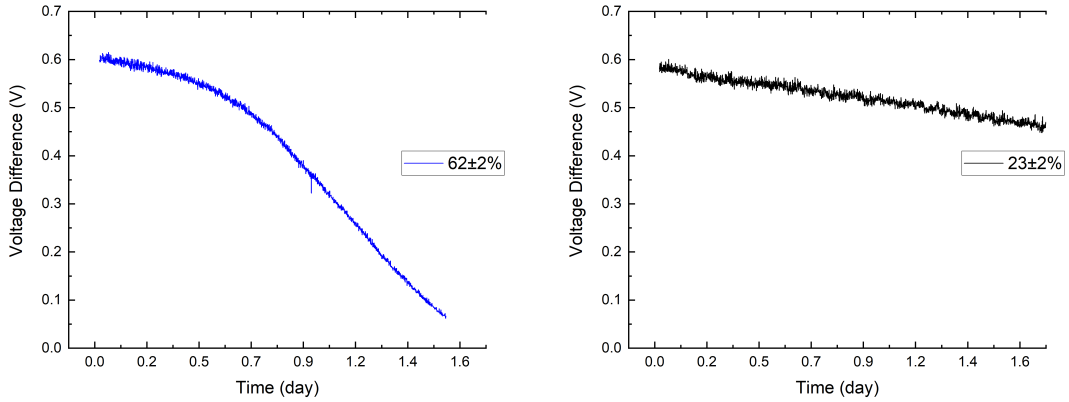

(a) (b)

Figure 3.3: The change in voltage difference in each measurement with respect to time. Image (a) shows the change in 62% RH. Image (b) shows the change in 23% RH. The voltage difference decays at an increasing rate at 62%. At 23%, the decay is more stable. The small fluctuation are caused by thermal noise.

As Figure 3.3 shows, the charge decreases faster at 62.45% RH than at 23.46%. The slope of the plot at 62.45% also decreases faster. To further compare the differences in the discharging process, we plot the change in voltage difference under 5 different relative humidities in Figure 3.4. For each humidity, we normalize the voltage difference by its initial value. To reduce the noise in the data, we take the average value of every 10 consecutive data values.

The charge decays much faster at high humidity than low humidity. Moreover, the discharging process varies between high and low humidities. At high humidity (62.45%, 75.29%), the slope of the curve decreases rapidly. At low humidity (17.26%, 23.46%, 49.92%), the slope of the curve tends to be constant.

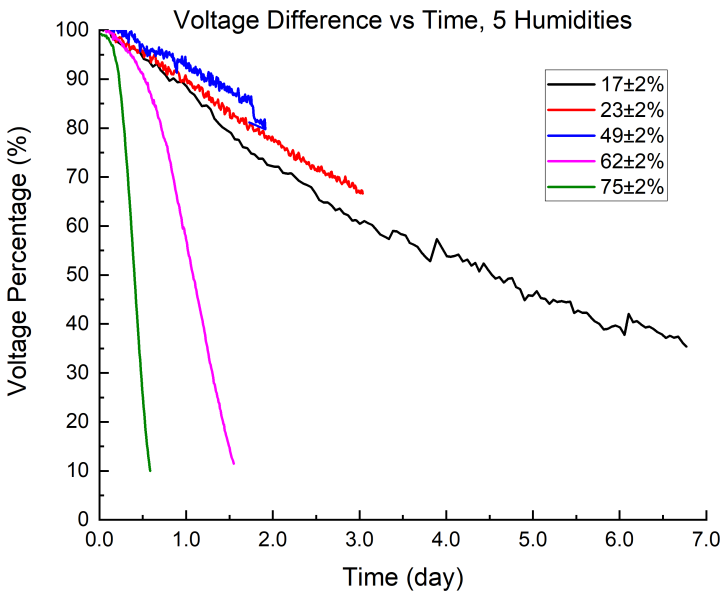

Figure 3.4: Voltage difference with respect to time for 5 different values of RH. The total measurement time in experiment is different for each curve. At high humidities, as humidity increases, the voltage decreases faster. At low humidities, the voltage decreases much slower than at high humidities.

In Figure 3.4, the slope of the curve at high humidity first experiences a slow decay, then decreases rapidly, but when approaching 10%, the slope tends to increase. For the curve at low humidity, the slope also varies as time progresses. As discussed later in section 4.2.1, the discharge behavior depends on the remaining charge on the particle. Tada and Murata found that the voltage decreases exponentially [9]. In our experiment, rather than simple exponential decay, the curve experiences a step change. Thus, we fit the data to a logistic form, as given by

$$V(t) = \frac{A}{1 + e^{\alpha(t - t_h)}} \tag{3.1}$$

to the curve. The curve fitting MATLAB code is provided by James Conder [18]. In Equation (3.1), $V(t)$ represents the value of voltage difference with respect to time; A is the maximum value of the logistic equation; α is the logistic growth rate of $V(t)$; t_h is the t-value of the

symmetric inflection point.

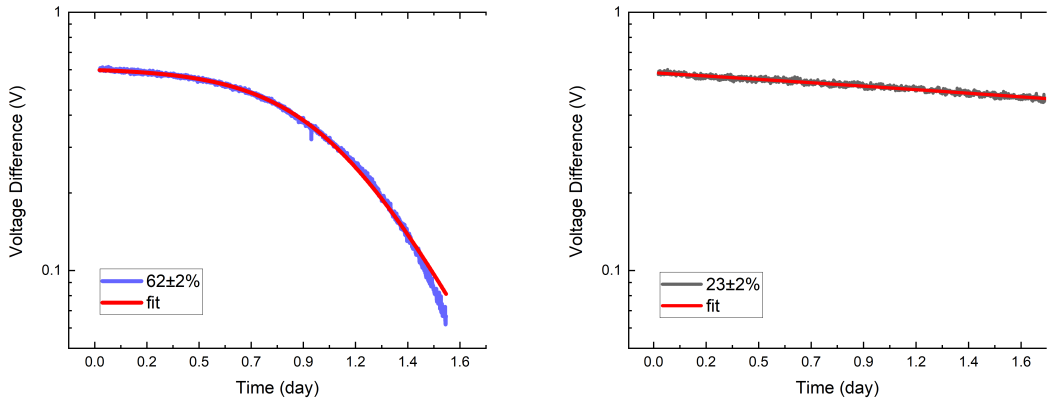

(a) (b)

Figure 3.5: The logistic fitting result of the sample curves in Figure 3.3. Image (a) shows the change in voltage difference in 62% RH. Image (b) shows the change in voltage difference in 23% RH. The voltage difference is plotted in logarithmic scale. The nonlinear curve fitting result at 62% indicates that the change voltage difference is not an exponential decay.

Figure 3.5 shows the logistic curve-fitting result of two sample measurements given in Figure 3.3. The voltage difference is plotted in logarithmic scale. Unlike exponential decay, where the decaying curve is a straight line in logarithmic scale, the 62% RH shows a clear logistic behavior. The 23% curve can still be fitted, but it's uncertain whether the general behavior of the data is logistic or not.

We define $\tau = 1/\alpha$ as the time constant of Equation (3.1). τ represents a time scale at which $V(t)$ decreases.

For a polystyrene bead, we measure the change in voltage difference with respect to time under 33 different RH values, fit the data with Equation (3.1) to find the constant coefficients (A,α,t_h), and calculate the time constant τ for each measurement.

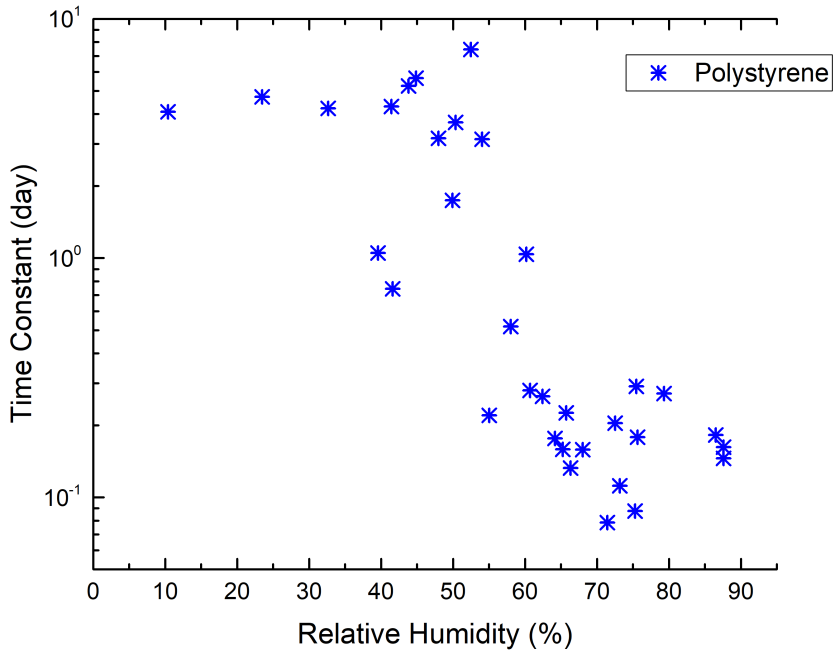

Figure 3.6: Time constant vs relative humidity. The time constant is displayed in logarithmic scale. Each data point is obtained from a fitting to a single voltage difference curve at a specific RH.

Figure 3.6 shows the value of the time constant τ of the logistic curve fitting result for each humidity. In the low humidity region (below 45%), the time constant stays at around 5 days. In the medium humidity region (45% to 55%), the time constant decreases significantly as humidity increases. In the high humidity region (above 55%), the time constant stabilizes at around 0.2 day.

To further investigate the principles behind the discharging process, we change the surface property of the polystyrene bead. We use a thermal evaporator to coat the bead with a thin layer of gold. In this way, we change the bead's surface conductivity as well as the chemical nature of the surface's interaction with water. We calculate the time constant τ for 27 voltage difference curves. Each curve represents a single measurement of the change in voltage difference with respect to time at a specific RH.

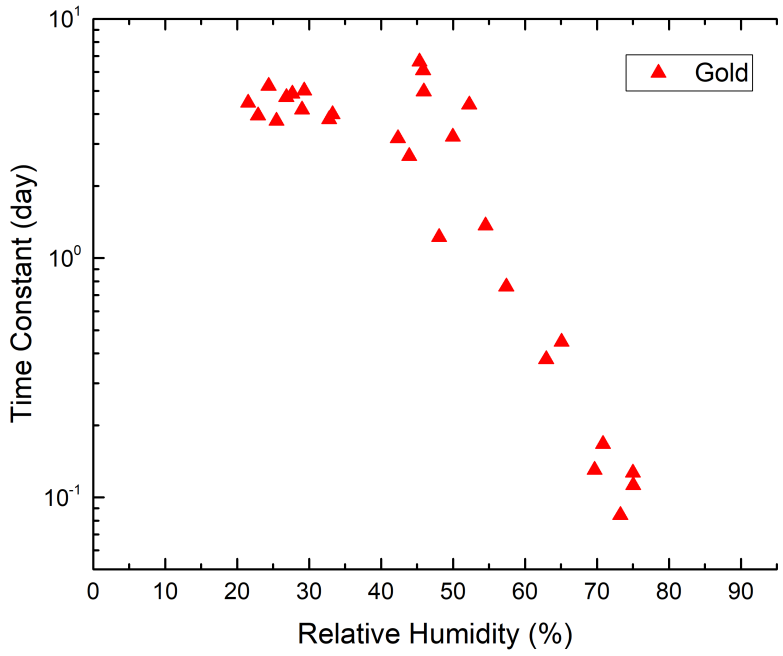

Figure 3.7: Time constant vs relative humidity for gold bead. Time constant is displayed in logarithmic scale. The RH varies from 20% to 76%. The change in time constant with respect to RH shows a similar behavior as Figure 3.6.

As Figure 3.7 shows, for the gold bead, the change in the time constant τ with respect to relative humidity follows a similar pattern to that of the polystyrene bead.

Chapter 4

Discussion

4.1 Pressure variation

In Table 3.1, the density and mean minimum falling pressure of pumice are both approximately five times larger than the corresponding values of the polystyrene beads. This result is consistent with Equation (1.10). For two spherical particles of the same size, an increase in density is represented by an increase in mass. Equation (1.10) shows that with regards to particle properties, the acoustic radiation force is only affected by the particle radius a. Thus the radiation force will be the same for both the pumice and the polystyrene bead. Meanwhile, the gravitational force on the particle will vary, since particle's mass is different.

From Equation (1.11), the maximum radiation force is proportional to the density of air ρ_0. From Equation (1.14), the density of air is proportional to the air pressure inside the chamber. Therefore, the minimum pressure required to levitate the particle by overcoming the particle's gravitational force is proportional to the density of the particle, as shown in Equation (1.13).

From Figure 3.1, we do not observe a dependence of the minimum air pressure on the number of beads. The variation between the minimum air pressure values for each number of beads may

due to the arrangement of the particles. As the number of beads increases, the beads are clustered together in the same horizontal plane inside the levitator. The nodes of the standing sound wave are concentrated in a small region. As the number of beads increases, the cluster size reaches out of the region, causing the radiation force to be unevenly distributed.

4.2 Charge measurement

As Figure 3.3 indicates, the discharging behavior of polystyrene bead varies between low and high humidity. The charge on the polystyrene bead decreases more rapidly at high humidity than at low humidity.

Figure 3.4 shows the discharging behavior of polystyrene beads for values of five different humidity. At high humidity, the discharging process is better represented by a logistic curve rather than an exponential curve. Moreover, at high humidity, the discharging process is more sensitive to variation in humidity. At low humidity, the effect is not obvious. The change in humidity influences the discharging behavior at low humidity, but it's not the dominant factor.

The charge decreases much slower at low humidity. The charge on the polystyrene bead can last for weeks at low humidities (Figure 3.4, 17% RH). At high humidity the charge decays by 90% in only one or two days.

Figure 3.4 indicates that there exists two types of discharging mechanism at low and high humidity. Humidity dominates the discharging process at high humidities. The main charge transfer may be achieved by the interaction between the negative charge on the polystyrene beads and the water molecules in the environment. At low humidity, the bombardment of air molecules on the polystyrene bead may account for the discharging process.

4.2.1 Discharge behavior at high humidities

After fitting Equation (3.1) to each discharging curve and calculating the time constant, we obtain Figure 3.5. The influence of humidity is beginning to be significant between 40% and 60%. This is the range where humidity begins to play a major role in the discharging process.

Equation (3.1) is well-fitted to voltage difference data measured at high humidity. For an exponentially decaying curve, the decay rate decreases exponentially with time, causing the entire discharge process to gradually slow down. However, for a logistically decaying curve, the charge decreases slowly at the beginning and the end, but decreases exponentially in the middle. Such a good fit to an equation of logistic form likely indicates a complex discharge process. We hypothesize that the logistic behavior indicates a two-step charge loss mechanism.

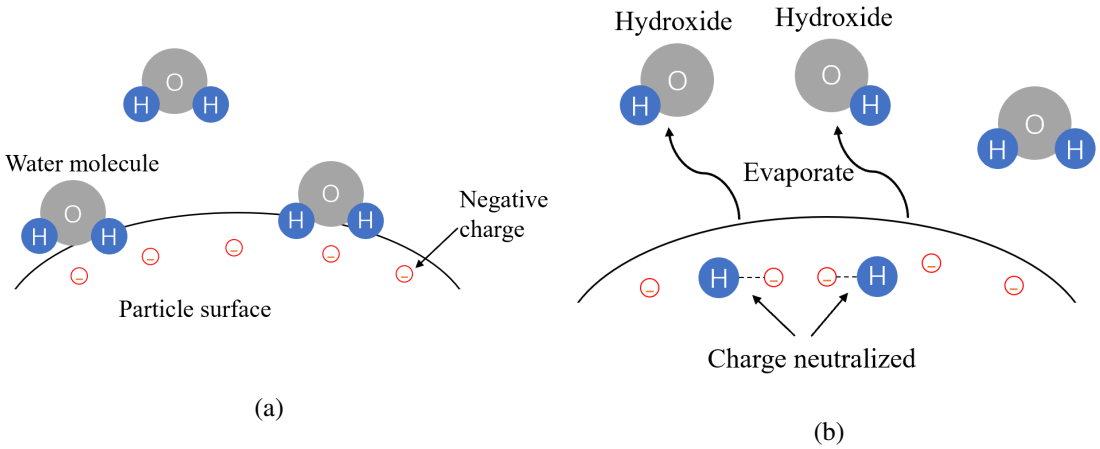

Figure 4.1: Demonstration of the two-step charge loss process at high humidities. Image (a) shows the adherence of water molecules to particle's surface. Image (b) shows the neutralization of negative charge on the particle.

Figure 4.1 demonstrates the two-step mechanism. In the first step, the water molecules in air adhere to the particle's surface. In the second step, the positive hydrogen ion neutralizes the negative charges on the particle's surface; then the remaining hydroxide ions evaporate away. Both steps may contribute to the logistic behavior of the discharge process. In the first step, the

humidity may affect the rate of water molecules adhering to the bead's surface [19][20][21][22]. In the second step, the environmental humidity may influence the neutralization and evaporation processes [23].

In Figure 3.6, at around 45% relative humidity, the influence of humidity starts to dominate the discharge process. The increase in humidity speeds up the two-step charge loss process, and the time constant decreases rapidly with relative humidity. We also notice that at very high humidity (65% and above), the rate of change of the time constant slows down with respect to relative humidity. In this case, the water molecules on the surface may be saturated, and the humidity will no longer be the major influencing factor.

Our lab member Jake McGrath uses the quartz crystal microbalance (QCM) to measure the thickness of the water layer with respect to RH. QCM detects the change in frequency of a quartz crystal resonator and measures the variation of mass per unit area. The QCM is placed inside a chamber. The mixture of water vapor and dry air flows into the chamber from the top. The humid air forms water layer on the QCM surface. We then measure the change in QCM's frequency and calculate the thickness of the water layer with respect to RH inside the chamber.

Figure 4.2 shows the change in water layer's thickness with respect to RH. The thickness of the water layer rapidly increases after 45% RH. This is consistent with Figure 3.6, where the time constant rapidly decreases after 45%. Such behavior in the change of water layer with respect to RH provides strong evidence that the water dissociation plays a critical role in the discharging process at high humidity.

4.2.2 Discharge behavior at low humidities

At low humidity, the humidity makes a negligible contribution to the discharge process. We hypothesize that the main influencing factor at low humidity is the collision rate between the

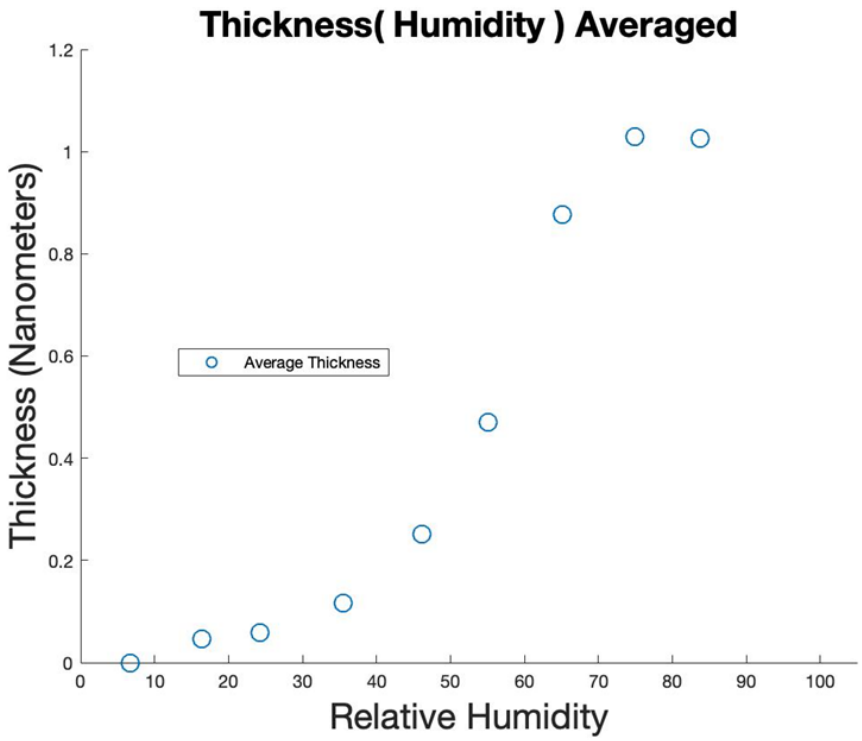

Figure 4.2: Change in water layer's thickness with respect to RH. Each data point is the average thickness of three measurements. The thickness beings to grow rapidly at approximately 45% RH.

particle and air molecules. As air molecules collide with the charged particle, the charge may be transferred to the air molecules by conduction. The air molecules may also be triboelectrically charged. Changing the air pressure will change the density of air, and thus influence the collision rate of the air molecules. Taking charge measurements at various pressures at low humidity will be our future investigation.

4.2.3 Effect of particle composition on discharge behavior

To test the influence of particle composition, and especially conductivity, on the discharging process, we perform the experiments on gold beads. As Figure 4.3 shows, there are no major differences between the time constants of polystyrene and gold as humidity varies. This result

indicates that the conductivity does not play a major role in the discharge process.

As the two-step process in section 4.2.1 describes, the water molecules first adhere to the particle's surface, then neutralize the charge. Therefore, the hydrophobicity of the particle may also influence the discharge behavior. For example, water molecule may be less likely to attach to the particle surface if the particle is highly hydrophobic. In this case, the discharge process would slow down even at high humidities.

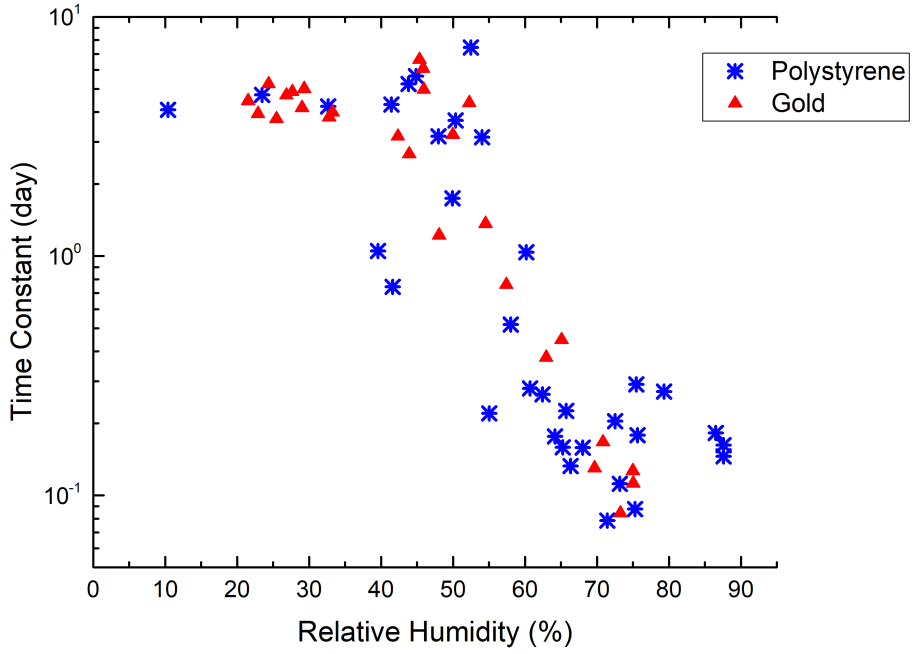

Figure 4.3: Comparison of time constant between polystyrene and gold. The change in time constant with respect to RH shows no significant differences between polystyrene and gold particles.

Chapter 5

Conclusions and Future Work

We test the performance of the acoustic levitator with respect to change in environmental pressure and particle density with polystyrene particles and pumice. As pressure decreases, the acoustic radiation force decreases. For particles with the same size, denser particles are more difficult to levitate. Using the built acoustic levitator, we measure the discharging process and its time constant for polystyrene and gold particles under different humidity conditions. For each measurement in a specific humidity, we fit the logistic equation to the data of the measured voltage change with respect to time. We calculate the time constant for each data set and plot it with respect to relative humidity. From the data, we discover that the discharge rate increases rapidly after 40% relative humidity. At high humidity, the discharging curve behaves logistically; the charge decrases at a timescale of hours. At low humidity, the timescale for discharge is weeks. This reveals that there may be two separate discharge mechanisms: one for the low and another for the high humidity discharging process. We also test the discharging behavior of the polystyrene bead with gold-coated surface. Comparing the change of the time constant with respect to time between polystyrene and gold, we find no major differences. Thus, the composition of the particle does not play a major role in the discharging process.

Future investigations will focus on the following aspects:

- Record the entire discharging process for polystyrene at low humidity. As Figure 3.4 shows, at low humidity the discharging process has a timescale of weeks. Measuring only the initial discharging behavior may not fully represent the general discharging trends. Thus we need a complete measurement of the entire discharging process to further analyze the behavior.

- Change the air composition in the chamber. The water molecules in air may be responsible for charge transportation between the particle and the environment, especially at high humidity. Introducing other molecules in the air, such as alcohol, can help to examine the role of water in the discharging process.

- Perform charge measurements at low humidity and vary the air pressure. We hypothesized that at low humidity, the charge is mainly lost due to collisions with air molecules. By varying the air pressure inside the chamber, we can test our hypothesis and further investigate how low humidity affects the discharging behavior.

Bibliography

[1] Keith M Forward, Daniel J Lacks, and R Mohan Sankaran. Particle-size dependent bipolar charging of martian regolith simulant. *Geophysical Research Letters*, 36(13), 2009.

[2] AA Mills. Dust clouds and frictional generation of glow discharges on mars. *Nature*, 268(5621):614–614, 1977.

[3] H Frank Eden and Bernard Vonnegut. Electrical breakdown caused by dust motion in low-pressure atmospheres: Considerations for mars. *Science*, 180(4089):962–963, 1973.

[4] Sarah J Snyder, Paul E Hintze, Judith L McFall, Charles R Buhler, J Sid Clements, and Carlos I Calle. Triboelectric charging of dust and its relation to organic degradation on mars. In *Proceedings of the ESA Annual Meeting on Electrostatics*, 2008.

[5] Troy Shinbrot, Keirnan LaMarche, and Benjamin J Glasser. Triboelectrification and razorbacks: geophysical patterns produced in dry grains. *Physical review letters*, 96(17):178002, 2006.

[6] Sushil K Atreya, Ah-San Wong, Nilton O Renno, William M Farrell, Gregory T Delory, Davis D Sentman, Steven A Cummer, John R Marshall, Scot CR Rafkin, and David C Catling. Oxidant enhancement in martian dust devils and storms: implications for life and habitability. *Astrobiology*, 6(3):439–450, 2006.

[7] MR James, L Wilson, SJ Lane, JS Gilbert, TA Mather, RG Harrison, and RS Martin. Electrical charging of volcanic plumes. *Space Science Reviews*, 137(1-4):399–418, 2008.

[8] Rafael Navarro-González, Mario J Molina, and Luisa T Molina. Nitrogen fixation by volcanic lightning in the early earth. *Geophysical Research Letters*, 25(16):3123–3126, 1998.

[9] Yasufusa Tada and Yuji Murata. Direct charge leakage through humid air. *Japanese journal of applied physics*, 34(4R):1926, 1995.

[10] Daniel J Lacks and R Mohan Sankaran. Triboelectric charging in single-component particle systems. *Particulate Science and Technology*, 34(1):55–62, 2016.

[11] Shuji Matsusaka, H Maruyama, T Matsuyama, and M Ghadiri. Triboelectric charging of powders: A review. *Chemical Engineering Science*, 65(22):5781–5807, 2010.

[12] Henrik Bruus. Acoustofluidics 7: The acoustic radiation force on small particles. *Lab on a Chip*, 12(6):1014–1021, 2012.

[13] K Yasuda and T Kamakura. Acoustic radiation force on micrometer-size particles. *Applied physics letters*, 71(13):1771–1773, 1997.

[14] M Barmatz and P Collas. Acoustic radiation potential on a sphere in plane, cylindrical, and spherical standing wave fields. *The Journal of the Acoustical Society of America*, 77(3):928–945, 1985.

[15] Mark Senn. *Acoustic Levitator : 26 Steps (with Pictures) - Instructables*, 2017 (accessed March 25, 2020). `https://www.instructables.com/id/Acoustic-Levitator/`.

[16] Asier Marzo, Adrian Barnes, and Bruce W Drinkwater. Tinylev: A multi-emitter single-axis acoustic levitator. *Review of Scientific Instruments*, 88(8):085105, 2017.

[17] A Marzo, A Ghobrial, L Cox, M Caleap, A Croxford, and BW Drinkwater. Realization of compact tractor beams using acoustic delay-lines. *Applied Physics Letters*, 110(1):014102, 2017.

[18] James Conder. $fit_logistic(t,Q),2010(accessedApril10,2020).$ $https$: $//www.mathworks.com/matlabcentral/fileexchange/41781-fit_logistic-t-q.$

[19] NJ Mills and P Kang. The effect of water immersion on the mechanical properties of polystyrene bead foam used in soft shell cycle helmets. *Journal of cellular plastics*, 30(3):196–222, 1994.

[20] IY Gnip, V Kersulis, S Vejelis, and S Vaitkus. Water absorption of expanded polystyrene boards. *Polymer testing*, 25(5):635–641, 2006.

[21] Daneti Saradhi Babu, K Ganesh Babu, and Wee Tiong-Huan. Effect of polystyrene aggregate size on strength and moisture migration characteristics of lightweight concrete. *Cement and Concrete Composites*, 28(6):520–527, 2006.

[22] Bernd Winter, Manfred Faubel, Robert Vácha, and Pavel Jungwirth. Behavior of hydroxide at the water/vapor interface. *Chemical Physics Letters*, 474(4-6):241–247, 2009.

[23] AV Shavlov, VA Dzhumandzhi, and AA Yakovenko. Charge separation at the evaporation (condensation) front of water and ice. charging of spherical droplets. *Technical Physics*, 63(4):482–490, 2018.